VO_2-Based MEMS Mirrors

David Torres, *Student Member, IEEE*, Tongyu Wang, Jun Zhang, *Student Member, IEEE*, Xiaoyang Zhang, Sarah Dooley, Xiaobo Tan, *Senior Member, IEEE*, Huikai Xie, *Senior Member, IEEE*, and Nelson Sepúlveda, *Senior Member, IEEE*

***Abstract*— This paper reports the integration of vanadium dioxide (VO_2) thin films in a microelectromechanical systems (MEMS) mirror device, where the actuation is mainly due to the solid–solid phase transition of VO_2. The fabrication process described in this paper provides the details that will enable the integration of VO_2 thin films at any step during the fabrication of rather complex MEMS devices. The present VO_2-based MEMS mirror device is operated electro-thermally through integrated resistive heaters, and its behavior is characterized across the phase transition of VO_2, which occurs at a temperature of ∼68 °C and spans about 10 °C. The maximum vertical displacement of the mirror platform is 75 μm and it occurs for an input voltage of 1.1 V. This translates to an average power consumption of 6.5 mW per mirror actuator and a total power consumption of 26.1 mW for the entire device. The studies included in this paper are key for future device improvements and further development of MEMS mirror actuation technology, which could include the use of the hysteresis of VO_2 for programming tilting angles in MEMS mirrors. [2016-0016]**

***Index Terms*— Microelectromechanical systems (MEMS)-mirrors, vanadium dioxide, phase-change materials.**

I. Introduction

MICROELETROMECHANICAL mirrors have demonstrated to be useful components for systems in multiple fields, including optical displays [1], [2], phase arrays [3], [4] spectroscopy [5], medical imaging [6]–[8], optical switches [9], track-positioning [10], scanners [11], and microscopy [12]. Given the broad spectrum of areas where MEMS mirror devices are found useful, it is difficult to define a single figure of merit that universally describes the performance of a MEMS mirror. For example, large deflections and tilting angles are very important for increasing the field of view of MEMS mirrors used in microendoscope and tracking applications, while low voltage operation allows for reducing power consumption of devices used in scanning mirrors used for imaging. Although it can be argued that increasing displacements/tilting angles and decreasing power consumption will result in better MEMS mirrors, the technologies that have been used for these devices do not include a single mechanism that can optimize both [13].

The techniques that have been used for actuation of MEMS mirrors include bimorph, electrostatic, electromagnetic, and piezoelectric mechanisms. Bimorph mechanisms involve the use of two materials (in the form of thin films) with different thermal expansion coefficients. A change in temperature will produce different expansions of the layers forming the bimorph, causing bending of the bimorph structure [14]. This mechanism is known to produce very large deflections (and tilting angles) in MEMS mirrors, but such deflections require larger current signals, which translates into high power consumption. Furthermore, being a thermal process, their responses are relatively slow. Electromagnetic actuation requires magnetic materials and also requires relatively large currents; for example, 515.17mA was used to actuate the MEMS mirror based on electromagnetic mechanism [15]. Electrostatic mechanisms, on the other hand, use the attractive (or repelling) force between two charged plates or surfaces, which requires very little current, and therefore, consume low power. When they are fabricated in the micrometer scale, they can sustain very high electric fields since the gaps between the charged surfaces can be smaller than the mean free path of particles in air at room temperature (∼6 μm) [16]. Similarly, piezoelectric actuation mechanisms require very small currents, and are capable of providing high-speed actuation [17]. However, the work-per-unit volumes of electrostatic and piezoelectric actuation mechanisms are about one order of magnitude smaller than of thermal expansion [18], which yields smaller deflections and tilting angles for similar devices.

This work presents a new actuation mechanism for MEMS mirrors. The mechanism consists of the stress generated by vanadium dioxide (VO_2) thin films during their solid-solid phase-change. During its phase transition, VO_2 experiences a fully reversible solid-to-solid phase transformation, in which the electrical [19], optical [20] and mechanical [21] properties drastically change. The mechanical properties involve a decrease in the area of the thin film crystals that are parallel to the substrate. This generates stress levels close to 1 GPa [22] and strain energy densities close to $10^6\,\mathrm{J\,m^{-3}}$, which is close

Manuscript received February 4, 2016; revised April 1, 2016; accepted April 10, 2016. Date of publication May 18, 2016; date of current version July 29, 2016. This work was supported in part by the National Science Foundation under Grant CMMI 1301243 and Grant ECCS 1306311, and in part by the Device Development Cooperative Research and Development Agreement within the Air Force Research Laboratory Sensors Directorate and Michigan State University under Grant 15-075-RY-01. Subject Editor C. Hierold.

D. Torres, T. Wang, X. Tan, and N. Sepúlveda are with the Department of Electrical and Computer Engineering, Michigan State University, East Lansing, MI 48840 USA (e-mail: torresd5@egr.msu.edu; wangton3@msu.edu; xbtan@egr.msu.edu; nelsons@egr.msu.edu).

J. Zhang is with the Department of Electrical and Computer Engineering, University of California at San Diego, La Jolla, CA 92093 USA (e-mail: j5zhang@ucsd.edu).

X. Zhang and H. Xie are with the Department of Electrical and Computer Engineering, University of Florida, Gainesville, FL 32611 USA (e-mail: xzhang292@ufl.edu; hkxie@ece.ufl.edu).

S. Dooley is with the Sensors Directorate, Air Force Research Laboratory, Wright-Patterson Air Force Base, OH 45433 USA (e-mail: sarah.dooley@us.af.mil).

Color versions of one or more of the figures in this paper are available online at http://ieeexplore.ieee.org.

Digital Object Identifier 10.1109/JMEMS.2016.2562609

to 1 order in magnitude larger than values for electrostatic or piezoelectric actuation [23]. Given the large work-per unit volume capability, memory capability, and small temperature window during which the phase transition occurs (typically not wider than 20°C), VO_2-based micro actuators have been studied extensively in recent years [24]–[28]. Furthermore, the behavior of VO_2 across the phase transition shows hysteresis, which has made possible the development of programmable MEMS actuators [29] and resonators [30]. Although there are multiple solid-solid phase transition materials, VO_2 is the material with phase transition temperature closest to room temperature [31] (approximately 68°C), which makes it a very attractive option for practical applications.

The hysteresis between deflection and temperature of VO_2-based actuators follows a non-monotonic behavior, which has been described before [22], [32] and is now briefly discussed. In VO_2-based actuators, the dominant mechanism for regions outside the phase transition, is the thermal expansion coefficient difference between VO_2 and the substrate material - just like in typical bimorph thermal actuators. During the phase transition, thermal expansion and phase transition mechanisms coexist and produce displacements in different directions; but the dominant mechanism is the stress generated by the change in the area of the VO_2 crystal due to the phase transition. Thus, the deflection of VO_2-based actuators follows a non-monotonic behavior when the device is heated from room temperature across the phase transition. VO_2-based mirrors also follow this distinct behavior during actuation.

The main contribution of this paper is the demonstration of a new thermal actuation mechanism for MEMS mirrors. Although VO_2-based MEMS actuators have been reported before [23], [24], [26], [29], [30], [32], [33], the monolithic integration of VO_2 thin films in rather complicated MEMS devices, such as MEMS mirrors, had not been demonstrated. The microfabrication process for the presented VO_2-based MEMS mirror is discussed in detail. The characterization of the device includes vertical displacement, tilting angle, dynamic response, and power consumption. When all the legs of the device are actuated simultaneously (generally referred to as the piston motion), the maximum displacement is 75 μm, which is obtained with an actuation voltage of 1.1 V for each leg.

II. Experimental Procedures

The developed VO_2-based MEMS mirror (SEM shown in Figure 1) is based on a previous design reported in [4], where the difference in the thermal expansion coefficient of aluminum and silicon dioxide (SiO_2) is replaced with VO_2 to generate deflections upon resistive heating. In this design, a squared mirror platform is suspended by 4 separate and individually-actuated legs. Each leg consists of different sections with two different thickness: a thin section with the two materials with different thermal expansion coefficients (bimorph) and a much thicker section that will provide a rigid frame that serves as a mechanical support (frame). This MEMS mirror design optimizes vertical displacement and its details have been reported [4], [34], [35]. Metal traces are embedded in the legs to form resistive heaters that are designed to increase the temperature mainly in the bimorph section of the leg (see Figure 1).

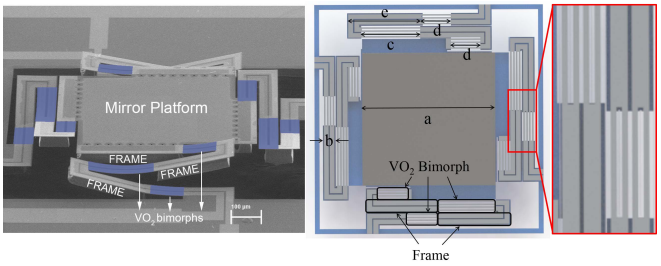

Fig. 1. (Left) SEM image of final device where the bimorph are colored on each leg, (right) Top view of VO_2-based MEMS mirror device (gray color represented the metal layer) with the following dimensions: a) 600 μm (platform), b) 62 μm (leg width), c) 300 μm (bimorph), d) 150 μm (bimorph) and e) 360 μm (frame).

A. Design and Fabrication of V O_2-Based MEMS Mirror

VO_2 thin films are not compatible with most standard microfabrication processes such as complementary metal-oxide semiconductor (CMOS) process. The CMOS process requires the use of very high temperature for different process such as SiO_2 deposition and ion diffusion. A high processing temperature will affect VO_2 thin films due to either film oxidation (i.e. change in materials stoichiometry) or possible diffusion of atoms from layers in contact with VO_2. Furthermore, CMOS devices that include aluminum as interconnect metals are sensitive to high processing temperatures. For example, a typical 0.25 μm CMOS technology cannot exceed temperatures higher than 475°C for 30 minutes [36]; VO_2 films are deposited at a temperatures of $\sim$ 470°C for 25 minutes and immediately followed by a 30 minutes annealing step. The material thin films also degrade rapidly when exposed to most etchants used in standard silicon MEMS processing, including some bases, such as concentrated AZ developers. This is why in the previously reported VO_2-based MEMS actuators, the deposition of the VO_2 film is done as the last step in the fabrication process [23], [26], [29], [30], [32], [33]. Although this approach can be done for relatively simple MEMS devices, it does not represent a viable solution for rather complicated structures, such as MEMS mirrors. Integrating VO_2 thin films at an early stage of a fabrication process requires the design of a fabrication process that does not involve high temperatures after the VO_2 is deposited, characterization studies of VO_2 thin films in the presence of unavoidable chemicals in lithography (e.g. photoresists and developers) and additional steps that protect the film during necessary wet-etching steps.

From preliminary experiments, it was found that after VO_2 thin films are brought to room temperature after the annealing step (VO_2 deposition process is explained later), they begin to degrade when exposed to temperatures above 275°C, in oxygen environment. It was also found that diluted developer solutions (i.e. 5:1 ; H_2O:Microposit 351) could be used to pattern photoresist layers on VO_2 and that any photoresist from the Microposit S1800 family and MicroChem SF-11 PMGI photoresist (with soft-baking of only 250°C) will not attack VO_2 thin films.

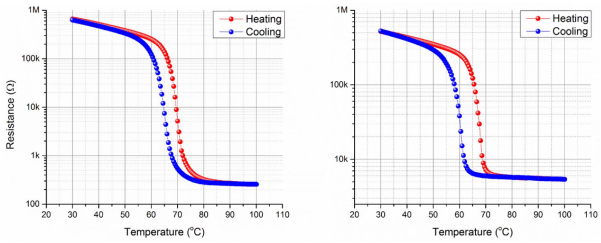

Fig. 2. Resistance drop across the phase transition for the VO_2 thin film right after its deposition (left), and after the MEMS mirror device is finalized (right).

The chip design included a device that allowed for measuring the resistance of the VO_2 thin film after the fabrication process was complete. The electrical properties can be used to characterize the quality of the VO_2 by measuring the resistance across the phase transition. Figure 2 shows the resistance drop of the VO_2 thin film right after the film was deposited, and after the fabrication process was completed. It can be noticed that both resistance drops show the characteristic drop in resistance (at similar temperature regions) and hysteretic behavior for a heating-cooling cycle across the phase transition of the material, which suggests that the composition of the VO_2 and its stoichiometry was not significantly affected during the process. That the difference in the resistance values before and after the transition is most likely due to the fact that the resistance drop shown in Figure 2-a was measured on a continuous VO_2 film, whereas Figure 2-b was measured on a patterned VO_2 patch (700 μm wide and 2.55 mm long) through the metal traces on the device.

The fabrication process flow diagram is presented in Figure 3. A double-side polished silicon wafer (2 inches in diameter and 300 μm thick) is used as a starting substrate. First, a 1 μm thick of SiO_2 layer is deposited by Plasma Enhanced Chemical Vapor Deposition (PECVD) at 300°C on both sides of the substrate. The SiO_2 layer is needed in one side (front side) for electrical insulation from the substrate and for growing polycrystalline strongly oriented VO_2 with the monoclinic $(011)_M$ planes parallel to the substrate surface [30], which will improve maximum mechanical actuation across the phase transition [29]. The SiO_2 on the back side of the wafer will be used as a hard mask for the back side silicon wafer etch. The next step is the deposition of the VO_2 film (250 nm thick), which is done by pulsed laser deposition following a similar process to that used previously for the development of VO_2-based MEMS [24]. The VO_2 film is patterned using S1813 as a mask, and Reactive Ion Etching (RIE). Table I shows the conditions used in the deposition and patterning of the VO_2. A 50 nm SiO_2 layer is then deposited to electrically isolate the patterned VO_2 and the resistive heaters (metal traces). This 50 nm SiO_2 layer is deposited at 250°C by PECVD, and in two consecutive steps (25 nm each deposition) to reduce voids in the film. It should be mentioned that the width of the VO_2 thin film is 2 μm smaller than the width of the bimorph lines. This is done to guarantee sidewall-protection of the VO_2 film by the SiO_2 layer (see step g of Figure 3).

TABLE I
CONDITIONS FOR RIE AND DEPOSITION OF VO_2

VO_2 RIE Etching		
Gas Flow (sccm)	He	50
	Ar	50
	SF_6	50
Power (W)		350
Pressure (mTorr)		20
VO_2 Deposition Conditions		
Gas Flow (sccm)	O_2	20
Temperature (°C)		470
Distance between sample and target (inches)		2
Pressure (mTorr)		15
Laser		
Energy (mJ)		350
Frequency (Hz)		10
Deposition Time (min)		25

The next step is the deposition and patterning of the metal traces, which is done by using lift-off technique. The metal traces are made of Titanium (Ti)/Platinum (Pt) (20 nm/110 nm), where the Ti layer is used for adhesion purposes. The width of the metal traces on the frames of the legs are 24 μm with a separation of 6 μm between the traces. In the bimorph region, the metal lines consist of two pairs of metal traces separated by 8 μm between the traces and 10 μm between the pair of traces. The width of each metal trace in the bimorph region is 6 μm (see the inset of Figure 1). After the metallization, another SiO_2 layer (150 nm) is deposited at 250°C; this time, where the deposition is divided into three steps of 50 nm each. This 150 nm SiO_2 layer is then patterned using dry etching to expose the metal contact pads and mirror platform. Another SiO_2 etch (1 μm) is performed to expose the silicon wafer for the release of the structure. The backside of SiO_2 is then patterned by RIE (1 μm) and used as a hard mask for the Deep Reactive Ion Etch (DRIE) on the silicon. During the backside etch, the top part of the wafer is protected with a dummy wafer using PMGA SF11 as adhesive layer between the wafers. The dummy wafer is removed by submerging the sample in photoresist remover (Microposit Remover 1165) at 90°C. The DRIE is timed to etch 250 μm of the silicon substrate, leaving approximately 50 μm of substrate, which is the thickness of the frame and platform in the final device. A second DRIE step is carried out on the top side of the wafer in order to complete etching through the wafer, leaving the entire MEMS mirror device suspended with a thickness of approximately 50 μm from the silicon substrate. Finally, to remove the 50 μm silicon under the bimorph sections, an isotropic Si etch was used (XeF_2 gas). The isotropic etch is timed to release the bimorph part of the legs, while not affecting significantly the silicon under the frame and platform sections of the MEMS mirror. The different sections of the final device are labeled in Figure 1.

B. Experimental Setup

The experimental setup is shown in Figure 4. A digital camera (Nikon 1 J1) with the combination of an objective lens (10X Mitutoyo Plan Apo Infinity Corrected Long

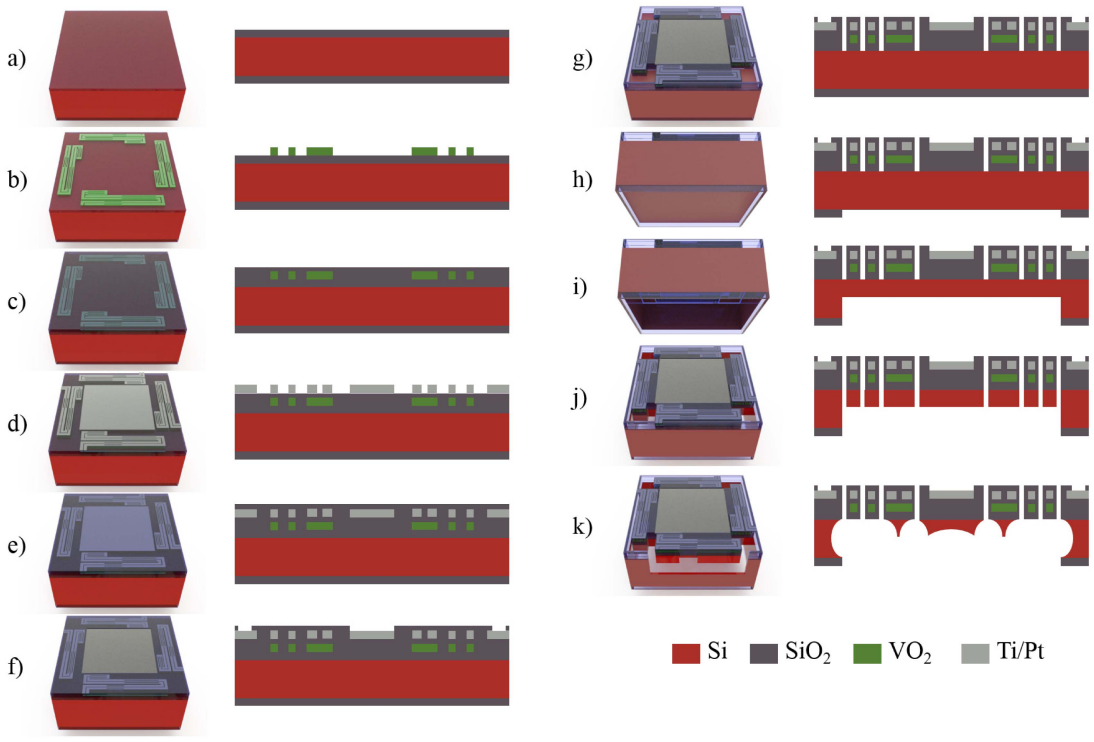

Fig. 3. Fabrication Process flow. a) PECVD of SiO_2, b) VO_2 deposition by PLD, c) PECVD of SiO_2 d) Metallization lift-off Ti/Pt, e) PECVD of SiO_2, f) opening to the metal contact pads (SiO_2 etch by RIE), g) SiO_2 etch by RIE, h) backside etch of SiO_2 by RIE, i) backside etch of Si (DRIE), j) SiO_2 etch by RIE, and k) Si isotropic etch (XeF_2).

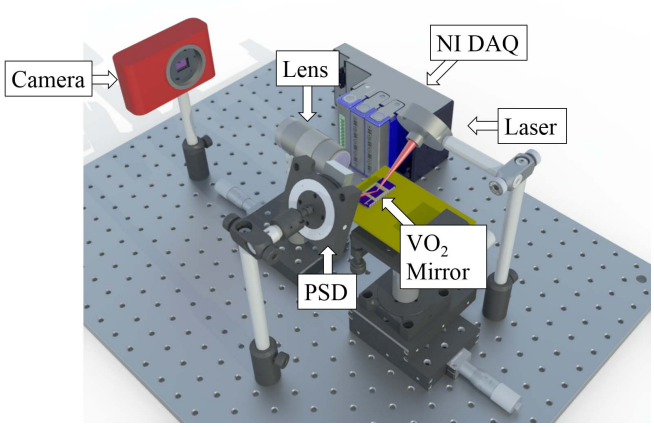

Fig. 4. Measurement setup used for characterization of VO_2 MEMS mirror.

WD Objective lens) was used to grab videos of the mirrors displacement with resolution of 0.7574 μm/pixel with a speed of 29.97 frame/second and 5 μm/pixel with a speed of 1200 frames per second. For better visualization of the dynamic behavior of the developed VO_2-based MEMS mirror, the authors have included supplementary color .avi file, which are available to download at http://ieeexplore.ieee.org. Tracker Video Analysis and Modeling software tool (Version 4.91, Douglas Brown, physlet.org/tracker) was used to analyze these images and videos. A data acquisition system (DAQ) from National Instrument controlled with LabView was used to provide actuation voltage to the resistive heaters. In order to automate the displacement measurements, an infrared (IR) laser ($\lambda = 985$ nm) and a 1-D position sensitive detector (PSD) were used to track the movement of the MEMS mirror platform due to the actuation of each leg (see Figure 4). However, since the laser was focused at the center of the platform, the displacement measured by the PSD did not represent the actual vertical displacement of the side of the platform closest to the leg that was being actuated. To compensate for this inaccuracy, the voltage reading from the PSD was calibrated with the maximum and minimum displacements of the platform sides, as recorded by the videos and Tracker software; i.e., Tracker software was used to calibrate the displacements measured by the PSD.

III. Results and Discussion

Different experiments were performed to characterize the performance of the presented MEMS mirror. The characterization included individual displacement of each leg, piston motion displacement, mirror tilting angle, and dynamic response.

A. Displacement and Tilting Angle Measurements

First, the displacement of the platform generated by the actuation of individual legs was measured using the IR laser and PSD (with calibration from Tracker software), with a voltage input to the resistive heaters that followed a sine wave: $V = 0.72\sin(2\pi f t) + 0.85$, where f is frequency (1 Hz), t is time, and 0.85 V represents an added offset voltage. The input signal was chosen to have the complete hysteresis loop with minimal distortion due to the frequency [33]. The sensing laser diode was directed on the mirror platform and had a power of 2.9 mW. Figure 5 shows the displacement

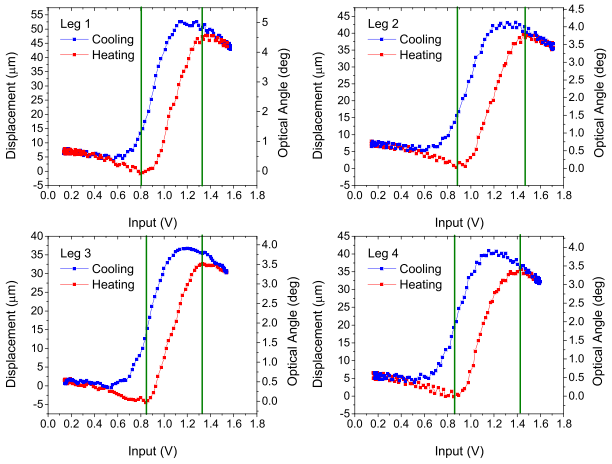

Fig. 5. Displacement for each individual mirror leg. Transition region of VO_2 occurs between the vertical lines.

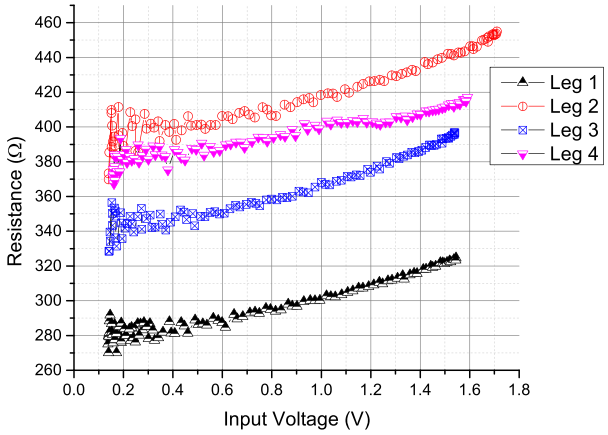

Fig. 6. Resistance of each heater traces as a function of voltage.

of the platform sides due to their corresponding leg. Every leg shows that the bending is in opposite directions for regions outside and inside the phase transition and this behavior is consistent with that of previously reported VO_2-based MEMS actuators. Furthermore, the hysteresis observed across the phase transition is not expected in systems where the dominant actuation mechanism is the difference in thermal expansion coefficient of two materials.

The tilting angle was calculated from the measurement of the displacement of each platform side for the actuation of the corresponding leg, using the following equation:

$$\theta = \sin^{-1}\frac{(h_1 - h_2)}{d},$$

where h_1 is the displacement of the platform side, h_2 is the displacement at the opposite side of the actuating leg (assumed to be 0 μm for no actuation), and d is the separation distance between h_1 and h_2, in this case the length of the platform mirror (600 μm) (see Figure 1).

Another observation from Figure 5 is that, although all the legs show similar displacement curves, their maximum/minimum displacement values are not the same, and they do not occur at the same voltage input. There are multiple possible reasons for this, but it has been verified that the most likely cause is related to the high sensitivity of VO_2-based actuators and the different temperature distributions in the heaters of each leg for the same current input. The hysteresis in the VO_2 film used for the present VO_2 based MEMS mirror spans only about 10°C (see Figure 2). Using the maximum vertical displacement measured, sensitivity can be estimated to be approximately 7μm/°C, or 169.95 μm V^{-1}. Given this sensitivity (which is significantly higher than that obtained with bimorph actuation [35]), any small difference between the structures of each leg (e.g., differences in structural thermal mass-due to underetching during release, or resistance of heaters-due to misalignments or lift-off process-) will result in different deflections for each leg for the same voltage input. To verify this hypothesis, the resistance of each heater was measured as a function of voltage. The result is shown in Figure 6, which shows the differences in resistance change with the same voltage input for the four heaters in each leg. It should be noted that Leg 1 shows the lowest resistance for the entire voltage range (see Figure 6). Thus, the dissipation of a specific power will require a lower voltage in Leg 1 than the other legs. Given the direct proportionality between heat and electric power; this implies that this Leg 1 require a smaller voltage in order to reach the same temperature than other legs. This behavior is verified in Figure 5, where Leg 1 shows the lowest voltage necessary to initiate the phase transition (0.8 V). The resistances of the other three Legs are much closer, and thus the difference in necessary voltage to initiate the phase transition is not that obvious for those three legs. This observation suggests that the responses of each leg could be synchronized by guaranteeing identical resistive heaters in each leg, and that the influence of structural differences between the legs due to underetching during the last step of the fabrication process is not very significant.

To measure the total displacement of the VO_2-based MEMS mirror, all the mirror legs were actuated at the same time, creating a piston movement. Just like for the actuation of individual legs, the input for the piston movement was an oscillating voltage, $V = 0.83\sin(2\pi f t) + 0.9$. This movement could not be measured using the 1-D PSD, since the reflected beam from the mirror platform did not follow a straight line; a voltage input value did not generate the same deflection in all mirror legs. Thus, the measurements for the piston movement had to be made using only the digital camera and a tracking software, and could not be automated. Figure 7 shows the vertical deflection of the mirror under piston movement. The largest vertical displacement is 75 μm, and it occurs when the voltage input to each leg is 1.1 V and within a change of input voltage of only 0.38 V. The correspondence between the voltage input and the mirror displacement is done by pairing the maximum of the voltage sine wave with the minimum in the mirror displacement after the phase transition is complete. This point occurs at approximately 1.25 s.

The difference in the input voltage needed to reach the maximum deflection between the individual (1.3-1.4V) and piston (1.1V) actuation can be caused by the difference in the extrinsic stress in the VO_2 thin films during actuation between both experiments. It is known that extrinsic stress can change the transition temperature of VO_2 [37].

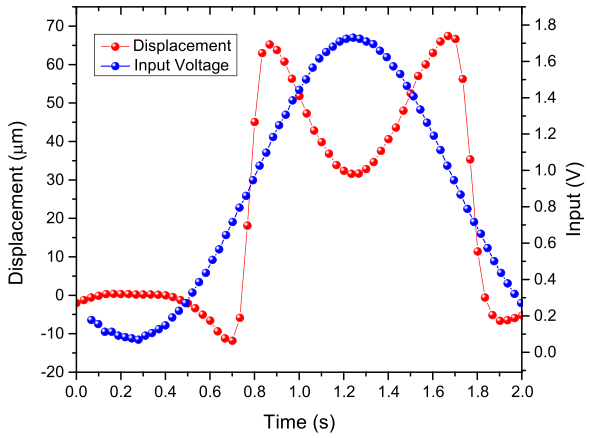

Fig. 7. Piston movement displacement (red), by actuating all the legs with the same input voltage (blue).

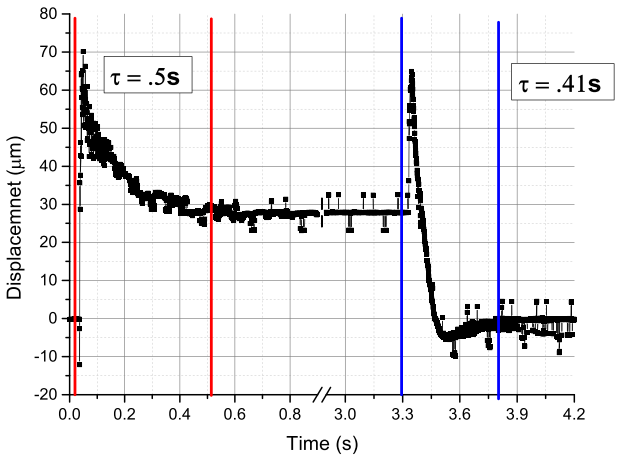

Fig. 8. Time response of the device with a piston like movement: red and blue lines indicate heating and cooling cycle, respectively.

During individual actuation, the lack of displacement from the other legs will restrain the movement of the actuated leg. Thus, when only one leg is actuated the net effect is an added stress to the VO_2 thin film. This added stress is lower when all the legs are actuated; notice that the larger maximum deflection measured for the piston movement (75 μm, shown in Figure 7) is larger than that obtained for individual actuation (ranging from 37 to 47 μm, shown in Figure 5). The non-monotonic behavior of each individual leg is reflected in the displacement curve for the piston actuation. Although the mirror platform is not expected to remain parallel during actuation since each leg does not show the same deflection for a given voltage input, this difference is not noticeable in the obtained videos (see supplementary information for videos). The dynamic response and power consumption studies discussed in the next section are based on this piston actuation.

B. Dynamic Response and Power Consumption

For the dynamic response of the present VO_2-based MEMS mirror, a step input that covered the entire phase transition for the four legs was applied. This guaranteed that the recorded vertical displacement of the mirror platform corresponded to the outer hysteresis loop of each leg. A voltage step of 1.7 V (maximum voltage used for the oscillating voltage used for the piston-like actuation) was applied simultaneously to every leg. Given the different resistance of the heaters, this voltage step produced different currents in each leg, which ranged from 4.9 mA (for leg 1) to 3.8 mA for leg 2. The voltage step input was held at 1.7 V for a few seconds, and then returned to 0 V. The intention of the rather long duty cycle was to check for response variations due to environment fluctuations or creep. The displacement due to the voltage input was measured with the digital camera. Figure 8 shows the measured response. The steady-state vertical deflection of the mirror platform was reached in 0.5 seconds during the heating cycle (i.e. when the voltage step input went from 0 to 1.7V), and 0.41 seconds during the cooling cycle (i.e. when the voltage step input went from 1.7 to 0 V). The overshoot observed in the heating cycle can be explained by the fact that pulse during the heating cycle crosses the entire phase transition region after approximately 0.07 seconds and thermal expansion mechanisms begin to dominate, where the deflection decreases with increasing temperature. The response showed no creep behavior or displacement variations during steady-state.

TABLE II
POWER CONSUMPTION FOR INDIVIDUAL AND PISTON ACTUATION FOR DIFFERENT INPUT RANGE

Input Range	Power Consumption (mW)				
	Individual Actuation (Leg)				Piston Actuation
	1	2	3	4	
0 - 1.7 V	7.56	6.44	6.00	6.11	26.11
Across the phase transition	3.85	3.30	2.47	3.37	12.99

The power consumption of the present VO_2-based device was calculated for the actuation of each individual leg across the entire phase transition, using the applied voltages shown in Figure 5, and the heater resistances shown in Figure 6. The average power consumption of each individual leg was 6.53 mW. The power consumption for each leg was also estimated for actuation due to the phase transition only (i.e. from lowest deflection to largest deflections in the heating curves). The results are shown in Table 2, which include also the power consumption for piston–like actuation (i.e. actuation of the 4 MEMS mirror actuators).

IV. CONCLUSION

A MEMS mirror actuated by the phase change in VO_2 has been demonstrated for the first time. Details for the monolithic integration of VO_2 thin films at early stages in the microfabrication process of MEMS mirrors are discussed. The deflection of the VO_2-based MEMS mirror shows non-monotonic hysteretic behavior, characteristic of the mechanical actuation in MEMS induced by the solid–solid phase transition of VO_2. The device performance shows maximum vertical displacements and tilting angles of approximately 75 μm and 5.5°, respectively. The devices maximum displacement occurs within a change in voltage of only 0.38 V.

Given the hysteretic behavior shown in the displacement of VO_2-based actuators, the presented MEMS mirrors allow for the programming of tilting angles and total vertical displacements. Thus, future continuation of this work will focus on developing programmable MEMS mirrors, and improving the device design to allow for larger displacement/tilting angle values, as well as better control of the device performance, especially across the phase transition of VO_2.

ACKNOWLEDGMENT

The authors wish to acknowledge the contributions of Dr. John L. Ebel for helpful discussions and technical assistance at the Air Force Research Laboratory, Wright-Patterson Air Force Base, OH. The fabrication of the MEMS Mirror was partially done at the Lurie Nanofabrication Facility at University of Michigan. The SEM images were taken at the Composite Materials and Structures Center at Michigan State University.

REFERENCES

[1] P. F. van Kessel, L. J. Hornbeck, R. E. Meier, and M. R. Douglass, "A MEMS-based projection display," *Proc. IEEE*, vol. 86, no. 8, pp. 1687–1704, Aug. 1998.

[2] A. D. Yalcinkaya, H. Urey, D. Brown, T. Montague, and R. Sprague, "Two-axis electromagnetic microscanner for high resolution displays," *J. Microelectromech. Syst.*, vol. 15, no. 4, pp. 786–794, Aug. 2006.

[3] U. Krishnamoorthy, K. Li, K. Yu, D. Lee, J. P. Heritage, and O. Solgaard, "Dual-mode micromirrors for optical phased array applications," *Sens. Actuators A, Phys.*, vols. 97–98, pp. 21–26, Apr. 2002.

[4] L. Wu, S. Dooley, E. A. Watson, P. F. McManamon, and H. Xie, "A tip-tilt-piston micromirror array for optical phased array applications," *J. Microelectromech. Syst.*, vol. 19, no. 6, pp. 1450–1461, Dec. 2010.

[5] L. Wu, A. Pais, S. R. Samuelson, S. Guo, and H. Xie, "A mirror-tilt-insensitive Fourier transform spectrometer based on a large vertical displacement micromirror with dual reflective surface," in *Proc. Int. Solid-State Sens., Actuators, Microsyst. Conf. (TRANSDUCERS)*, Jun. 2009, pp. 2090–2093.

[6] S. R. Samuelson, L. Wu, J. Sun, S.-W. Choe, B. S. Sorg, and H. Xie, "A 2.8-mm imaging probe based on a high-fill-factor MEMS mirror and wire-bonding-free packaging for endoscopic optical coherence tomography," *J. Microelectromech. Syst.*, vol. 21, no. 6, pp. 1291–1302, Dec. 2012.

[7] D. Wang *et al.*, "Endoscopic swept-source optical coherence tomography based on a two-axis microelectromechanical system mirror," *J. Biomed. Opt.*, vol. 18, no. 8, p. 086005, 2013.

[8] L. Liu, E. Wang, X. Zhang, W. Liang, X. Li, and H. Xie, "MEMS-based 3D confocal scanning microendoscope using MEMS scanners for both lateral and axial scan," *Sens. Actuators A, Phys.*, vol. 215, pp. 89–95, Aug. 2014.

[9] C. R. Giles, V. Aksyuk, B. Barber, R. Ruel, L. Stulz, and D. Bishop, "A silicon MEMS optical switch attenuator and its use in lightwave subsystems," *IEEE J. Sel. Topics Quantum Electron.*, vol. 5, no. 1, pp. 18–25, Jan. 1999.

[10] J. P. Yang, X. C. Deng, and T. C. Chong, "An electro-thermal bimorph-based microactuator for precise track-positioning of optical disk drives," *J. Micromech. Microeng.*, vol. 15, no. 5, p. 958, 2005.

[11] J.-C. Tsai and M. C. Wu, "Design, fabrication, and characterization of a high fill-factor, large scan-angle, two-axis scanner array driven by a leverage mechanism," *J. Microelectromech. Syst.*, vol. 15, no. 5, pp. 1209–1213, Oct. 2006.

[12] H. Ra *et al.*, "Three-dimensional *in vivo* imaging by a handheld dual-axes confocal microscope," *Opt. Exp.*, vol. 16, no. 10, pp. 7224–7232, 2008.

[13] L. Y. Lin and E. G. Keeler, "Progress of MEMS scanning micromirrors for optical bio-imaging," *Micromachines*, vol. 6, no. 11, pp. 1675–1689, 2015.

[14] A. Jain, H. Qu, S. Todd, and H. Xie, "A thermal bimorph micromirror with large bi-directional and vertical actuation," *Sens. Actuators A, Phys.*, vol. 122, no. 1, pp. 9–15, 2005.

[15] A. R. Cho *et al.*, "Electromagnetic biaxial microscanner with mechanical amplification at resonance," *Opt. Exp.*, vol. 23, no. 13, pp. 16792–16802, 2015.

[16] A. C.-L. Hung, H. Y.-H. Lai, T.-W. Lin, S.-G. Fu, and M. S.-C. Lu, "An electrostatically driven 2D micro-scanning mirror with capacitive sensing for projection display," *Sens. Actuators A, Phys.*, vol. 222, pp. 122–129, Feb. 2015.

[17] T. Naono, T. Fujii, M. Esashi, and S. Tanaka, "Non-resonant 2-D piezoelectric MEMS optical scanner actuated by Nb doped PZT thin film," *Sens. Actuators A, Phys.*, vol. 233, pp. 147–157, Sep. 2015.

[18] P. Krulevitch, A. P. Lee, P. B. Ramsey, J. C. Trevino, J. Hamilton, and M. A. Northrup, "Thin film shape memory alloy microactuators," *J. Microelectromech. Syst.*, vol. 5, no. 4, pp. 270–282, 1996.

[19] A. Zylbersztejn and N. F. Mott, "Metal-insulator transition in vanadium dioxide," *Phys. Rev. B*, vol. 11, no. 11, p. 4383, 1975.

[20] A. S. Barker, Jr., H. W. Verleur, and H. J. Guggenheim, "Infrared optical properties of vanadium dioxide above and below the transition temperature," *Phys. Rev. Lett.*, vol. 17, no. 26, p. 1286, 1966.

[21] N. Sepúlveda, A. Rúa, R. Cabrera, and F. E. Fernández, "Young's modulus of VO_2 thin films as a function of temperature including insulator-to-metal transition regime," *Appl. Phys. Lett.*, vol. 92, no. 19, p. 191913, 2008.

[22] A. Rúa, F. E. Fernández, and N. Sepúlveda, "Bending in VO_2-coated microcantilevers suitable for thermally activated actuators," *J. Appl. Phys.*, vol. 107, no. 7, p. 074506, 2010.

[23] E. Merced, X. Tan, and N. Sepúlveda, "Strain energy density of VO_2-based microactuators," *Sens. Actuators A, Phys.*, vol. 196, pp. 30–37, Jul. 2013.

[24] T. Wang, D. Torres, F. E. Fernández, A. J. Green, C. Wang, and N. Sepúlveda, "Increasing efficiency, speed, and responsivity of vanadium dioxide based photothermally driven actuators using single-wall carbon nanotube thin-films," *ACS Nano*, vol. 9, no. 4, pp. 4371–4378, 2015.

[25] J. Zhang, E. Merced, N. Sepúlveda, and X. Tan, "Optimal compression of generalized Prandtl–Ishlinskii hysteresis models," *Automatica*, vol. 57, pp. 170–179, Jul. 2015.

[26] E. Merced, D. Torres, X. Tan, and N. Sepúlveda, "An electrothermally actuated VO_2-based MEMS using self-sensing feedback control," *J. Microelectromech. Syst.*, vol. 24, no. 1, pp. 100–107, Feb. 2015.

[27] K. Liu, C. Cheng, Z. Cheng, K. Wang, R. Ramesh, and J. Wu, "Giant-amplitude, high-work density microactuators with phase transition activated nanolayer bimorphs," *Nano Lett.*, vol. 12, no. 12, pp. 6302–6308, 2012.

[28] J. Cao *et al.*, "Colossal thermal-mechanical actuation via phase transition in single-crystal VO_2 microcantilevers," *J. Appl. Phys.*, vol. 108, no. 8, p. 083538, 2010.

[29] R. Cabrera, E. Merced, and N. Sepúlveda, "A micro-electro-mechanical memory based on the structural phase transition of VO_2," *Phys. Status Solidi A*, vol. 210, no. 9, pp. 1704–1711, 2013.

[30] E. Merced, R. Cabrera, N. Dávila, F. E. Fernández, and N. Sepúlveda, "A micro-mechanical resonator with programmable frequency capability," *Smart Mater. Struct.*, vol. 21, no. 3, p. 035007, 2012.

[31] S. D. Ha, Y. Zhou, A. E. Duwel, D. W. White, and S. Ramanathan, "Quick switch: Strongly correlated electronic phase transition systems for cutting-edge microwave devices," *IEEE Microw. Mag.*, vol. 15, no. 6, pp. 32–44, Sep./Oct. 2014.

[32] R. Cabrera, E. Merced, and N. Sepúlveda, "Performance of electrothermally driven VO_2-based MEMS actuators," *J. Microelectromech. Syst.*, vol. 23, no. 1, pp. 243–251, Feb. 2014.

[33] E. Merced, X. Tan, and N. Sepúlveda, "Closed-loop tracking of large displacements in electro-thermally actuated VO_2-based MEMS," *J. Microelectromech. Syst.*, vol. 23, no. 5, pp. 1073–1083, Oct. 2014.

[34] H. Xie, "Vertical displacement device," U.S. Patent 6 940 630, Sep. 6, 2005.

[35] L. Wu and H. Xie, "A large vertical displacement electrothermal bimorph microactuator with very small lateral shift," *Sens. Actuators A, Phys.*, vols. 145–146, pp. 371–379, Jul./Aug. 2008.

[36] H. Takeuchi, A. Wung, X. Sun, R. T. Howe, and T.-J. King, "Thermal budget limits of quarter-micrometer foundry CMOS for post-processing MEMS devices," *IEEE Trans. Electron Devices*, vol. 52, no. 9, pp. 2081–2086, Sep. 2005.

[37] J. Cao *et al.*, "Extended mapping and exploration of the vanadium dioxide stress-temperature phase diagram," *Nano Lett.*, vol. 10, no. 7, pp. 2667–2673, 2010.

David Torres (S'15) received the B.S. degree in electrical and computer engineering from the University of Puerto Rico, Mayagüez, Puerto Rico, in 2012. He is currently pursuing the Ph.D. degree with the Department of Electrical and Computer Engineering, Michigan State University (MSU), East Lansing, MI, USA. He participated in a number of research projects, including a summer research internship at MSU as an undergraduate student, and the Air Force Research Laboratories at Wright-Patterson Air Force Base, Dayton, OH, as a graduate student. He has recently been awarded the SMART Scholarship.

His current research interests include design, fabrication, and implementation of microelectromechanical actuators and control of hysteretic systems.

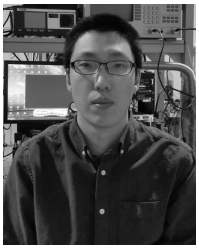

Tongyu Wang received the B.S. degree in electrical and computer engineering from the Beijing University of Aeronautics and Astronautics, Beijing, China, in 2010. He is currently pursuing the Ph.D. degree with the Department of Electrical and Computer Engineering, Michigan State University, East Lansing, MI, USA. He participated in numerous research programs, including as an Intern at Sony Mobile Communication AB, Beijing, in 2013; a Research Assistant at the National Key Laboratory of Science and Technology on Inertia, Beijing, from 2010 to 2013; and an Intern at the Baocheng Aviation Instrument Company Ltd., Baoji, China, in 2009.

His research interests include design, fabrication, and implementation of smart materials-based MEMS devices, and design, fabrication, and implementation of multilayer microfluidic system.

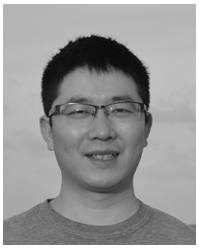

Jun Zhang received the B.S. degree in automation from the University of Science and Technology of China, Hefei, China, in 2011, and the Ph.D. degree in electrical and computer engineering from Michigan State University, East Lansing, MI, USA, in 2015. He is currently a Post-Doctoral Scholar with the University of California at San Diego, La Jolla, CA, USA. He received the Student Best Paper Competition Award at the ASME 2012 Conference on Smart Materials, Adaptive Structures, and Intelligent Systems, and the Best Conference Paper in Application Award at the ASME 2013 Dynamic Systems and Control Conference, and was named the Electrical Engineering Outstanding Graduate Student for 2014-2015.

His current research interests include modeling and control of smart materials, nonlinear system modeling and control for flexible robotics, and artificial muscles for robotics.

Xiaoyang Zhang received the B.S. degree from the Department of Electrical Engineering and Computer Science, Peking University, Beijing, China, in 2011. He is currently pursuing the Ph.D. degree with the Department of Electrical and Computer Engineering, University of Florida, Gainesville, FL.

His research interests include MEMS, optical MEMS, microactuators, micromirror, micro/nano fabrication, wide-angle laser scanning, and computer vision systems.

Sarah Dooley received the B.S. degree in physics from Xavier University in 2002, and the M.S. degree in electrooptics engineering from the University of Dayton in 2004. She is an Electronics Engineer with the Sensors Directorate, Air Force Research Laboratory, Wright-Patterson Air Force Base. She currently works in the field of non-mechanical beam-steering, including the design, fabrication, and characterization of MEMS micromirror arrays. She also collaborates with several institutions on the development of novel plasmonic and liquid crystal beam-steering techniques, MEMS optical switches, and MEMS frequency generation technology.

Xiaobo Tan (S'97–M'02–S'11) received the B.Eng. and M.Eng. degrees in automatic control from Tsinghua University, Beijing, China, in 1995 and 1998, respectively, and the Ph.D. degree in electrical and computer engineering from the University of Maryland, College Park, in 2002.

From 2002 to 2004, he was a Research Associate at the Institute for Systems Research, University of Maryland. He joined as a Faculty Member with the Department of Electrical and Computer Engineering, Michigan State University, in 2004, where he is currently a Professor. His research interests include modeling and control of systems with hysteresis, electroactive polymer sensors and actuators, and bio-inspired underwater robots and their application to environmental sensing.

Dr. Tan has served as an Associate Editor/Technical Editor of *Automatica*, the IEEE/ASME TRANSACTIONS ON MECHATRONICS, and the *International Journal of Advanced Robotic Systems*. He served as the Program Chair of the 2011 International Conference on Advanced Robotic, and the Finance Chair of the 2015 American Control Conference. He has co-authored one book entitled *Biomimetic Robotic Artificial Muscles* and over 70 journal papers, and holds one U.S. patent. He was a recipient of the NSF CAREER Award (2006), the MSU Teacher-Scholar Award (2010), and several best paper awards. He was named MSU Foundation Professor in 2016.

Huikai Xie (S'00–M'02–SM'07) received the B.S., M.S., and Ph.D. degrees from the Beijing Institute of Technology, Tufts University, and Carnegie Mellon University, respectively, all in electrical engineering. From 1992 to 1996, he was a Research Engineer at Tsinghua University, Beijing, China. He was at Bosch Corporation in 2001 and Akustica Inc. in 2002. He is currently a Professor with the Department of Electrical and Computer Engineering, University of Florida. He has published over 250 technical papers and holds 30 U.S. patents.

His research interests include MEMS/NEMS, CMOS-MEMS sensors, microactuators, integrated power passives, CNT-CMOS integration, optical MEMS, NIR/IR spectroscopy, and endoscopic optical imaging. He is a Senior Member of OSA.

Nelson Sepúlveda (S'05–M'06–SM'11) received the B.S. degree in electrical and computer engineering from the University of Puerto Rico, Mayagüez, Puerto Rico, in 2001, and the M.S. and Ph.D. degrees in electrical and computer engineering from Michigan State University (MSU), East Lansing, MI, USA, in 2002 and 2005, respectively. During the last year of graduate school, he attended Sandia National Laboratories as part of a fellowship from the Microsystems and Engineering Sciences Applications program.

In 2006, he joined as a Faculty Member the Department of Electrical and Computer Engineering, University of Puerto Rico. He was a Visiting Faculty Researcher at Air Force Research Laboratories (2006, 2007, 2013, and 2014), National Nanotechnology Infrastructure Network (2008), and the Cornell Center for Materials Research (2009); the last two being the National Science Foundation (NSF) funded centers at Cornell University, Ithaca, NY, USA. In 2011, he joined as a Faculty Member the Department of Electrical and Computer Engineering, MSU, where he is currently an Associate Professor. His current research interests include smart materials and the integration of such in microelectromechanical systems, with particular emphasis on vanadium dioxide thin films and the use of the structural phase transition for the development of smart microactuators.

Dr. Seplveda received the NSF CAREER Award in 2010 and the MSU Teacher Scholar Award in 2015.